

Theoretical and experimental studies for an orthopedic staple made up Nitinol

D. TARNITA*, D. BOLCU, C. BERCEANU, FL. CISMARU
University of Craiova, Faculty of Mechanics, Department of Applied Mechanics

Super-elastic NiTi has become a very important biomaterial, successfully used for technical and design issues relating to the miniaturization of medical devices and the increasing trend for less invasive and less traumatic procedures. In this paper, we present the elasticity matrix, the decomposition of the elasticity matrix, the eigenvalues and the eigenvectors for the crystallographic phases of Nitinol: trigonal, cubic, monoclinic and orthorhombic. In order to determine the variation law for the compression force developed by the Nitinol orthopaedic staple as function of temperature and, also, to validate the compression potential of the staple through constant pressure at the temperature of the human body, we made an experimental study, using an experimental stand. Using the video capture SIMI Motion software, the kinematical parameters of the both extremities of the staple were obtained. The analytical variation in time of the compression force exerted by the Nitinol staple is also obtained. The data acquired through this methods can be used to corroborate the experimental kinematical parameters with kinematical parameters obtained using various analytical or computer aided simulations in order to confirm a certain mechanical model.

(Received September 20, 2010; accepted November 19, 2010)

Keywords: Nitinol, crystallographic phases, spectral decomposition, experimental studies, orthopedic staple

1. Introduction

Shape memory alloys (SMA) constitute a group of metallic materials with the ability to recover a previously defined length or a shape when subjected to an appropriate thermo-mechanical load. When there is a limitation of shape recovery, these alloys promote high restitution forces. Because of these properties, there is a great technological interest in the use of SMA for different applications. Nitinol is a shape memory alloy containing approximately 50 at. % nickel and 50 at. % titanium and it is the alloy most frequently used in commercial applications because they combine good mechanical properties with shape memory effect.

Super-elastic NiTi has become a material of strategic importance as it allows to overcome a wide range of technical and design issues relating to the miniaturization of medical devices and the increasing trend for less invasive and therefore less traumatic procedures. The alloys have several advantages as greater ductility, more recoverable motion, excellent corrosion resistance, stable transformation temperatures, good kink resistance, less sensitivity to magnetic resonance imaging, fatigue life and the ability to be electrically heated for shape recovery [1–7] high biocompatibility [8-10]. These properties make it an ideal biological engineering material, especially in orthopedic surgery [11,12], orthodontics [13,14] neurosurgery [15], minimal invasive surgery [16], in vivo skin closure [17].

The form of the elasticity matrix contains the restrictions done by the symmetry theory of classical crystallography and it permits a simple geometrical interpretation of the relationship between stress and strain

regardless of the degree on anisotropy. These restrictions are reflected in the invariant structures of the spectral decompositions. The spectral forms are determined by the symmetry groups, and are independent of the values of the elastic constants.

The eigenvalues and eigenvectors of the elasticity tensor were first discussed in [18] by Kelvin and his results are summarized in the Encyclopedia Britannica (1878). More recently, in [19] and [20] the eigenvalues and eigenvectors for anisotropic elasticity were determined. In [21] Ting has discussed the eigenvalue problem in connection with his study of the invariants of the elasticity tensor. The strain energy function for anisotropic Elastic materials was presented in [22]

In these previous works, the elasticity tensor has been induced from a fourth-order symmetric linear transformation on the space of all 3x3 second-order tensors to a 6x6 second-order tensor.

The first spectral decomposition of the elasticity tensor was made in [23], using tensorial products. Then, Sutcliffe in [24] developed this method and they used it for different types of symmetries.

A more simple method, using matrix 6x6 was used in [25] for the decomposition of the rigidity matrix of the transversal isotropic materials.

2. Theoretical considerations

Be $[M]$ a symmetric matrix who belongs to $M_6(\mathcal{R})$.

So $[M] = [M]^t$. We can do for $[M]$ the following decomposition:

$$[M] = \lambda_1 [E_1] + \lambda_2 [E_2] + \dots + \lambda_m [E_m], m \leq 6 \quad (1)$$

where $\lambda_1, \lambda_2, \dots, \lambda_m$ are the eigenvalues of the matrix $[M]$. These values are determinate form the question:

$$\det[\lambda[I] - [M]] = 0 \quad (2)$$

and $[E_1], [E_2], \dots, [E_m]$ are matrix who belong to $M_6(\mathfrak{R})$ having the following properties:

$$[E_i][E_i] = [E_i] \quad (3)$$

$$[E_i][E_j] = [0] \quad i \neq j \quad (4)$$

$$[E_1] + [E_2] + \dots + [E_m] = [I] \quad (5)$$

The matrix $[E_i]$ can be determinate using the formula:

$$[E_i] = \sum_{k=1}^{h_i} [X][I_k][X]^t \quad (6)$$

where:

- h_i is the multiplying order of the proper value;
- $[I_k]$ is the matrix having on the principal diagonal in the position k the value 1 and all the order elements are null; $[I_k] \in M_6(\mathfrak{R})$;
- the matrix $[X]$ has the aspect:

$$[X] = [\bar{X}_1; \bar{X}_2; \bar{X}_3; \bar{X}_4; \bar{X}_5; \bar{X}_6] \quad (7)$$

Solving the following systems, we determine the components of the matrix $[X]$:

$$\begin{cases} [[M] - \lambda_k [I]] \bar{X}_k = 0 \\ x_{k_1}^2 + x_{k_2}^2 + \dots + x_{k_6}^2 = 1, \quad k = \overline{1;6} \end{cases} \quad (8)$$

where:

$$\bar{X}_k = \begin{bmatrix} x_{k_1} \\ x_{k_2} \\ \dots \\ x_{k_6} \end{bmatrix}, \quad k = \overline{1;6} \quad (9)$$

having the following property:

$$\bar{X}_k \cdot \bar{X}_j = \begin{cases} 1; & \text{if } k = j \\ 0; & \text{if } k \neq j \end{cases} \quad (10)$$

2.1. Decomposition of the elasticity matrix for Nitinol structure phases

In the case of the linear-elastic materials, the dependence between the deformation matrix components and the stress matrix components is a linear dependence:

$$\sigma_{ij} = \sum_{k=1}^3 \sum_{l=1}^3 S_{ijkl} \varepsilon_{kl} \quad (11)$$

This dependence can be written on the following form:

$$(\sigma) = [S](\varepsilon) \quad (12)$$

where:

$$(\varepsilon) = \begin{Bmatrix} \varepsilon_{11} \\ \varepsilon_{22} \\ \varepsilon_{33} \\ \sqrt{2} \varepsilon_{23} \\ \sqrt{2} \varepsilon_{13} \\ \sqrt{2} \varepsilon_{12} \end{Bmatrix}; \quad (\sigma) = \begin{Bmatrix} \sigma_{11} \\ \sigma_{22} \\ \sigma_{33} \\ \sqrt{2} \sigma_{23} \\ \sqrt{2} \sigma_{13} \\ \sqrt{2} \sigma_{12} \end{Bmatrix} \quad (13)$$

$$[S] = \begin{bmatrix} S_{1111} & S_{1122} & S_{1133} & \sqrt{2}S_{1123} & \sqrt{2}S_{1113} & \sqrt{2}S_{1112} \\ S_{2211} & S_{2222} & S_{2233} & \sqrt{2}S_{2223} & \sqrt{2}S_{2213} & \sqrt{2}S_{2212} \\ S_{3311} & S_{3322} & S_{3333} & \sqrt{2}S_{3323} & \sqrt{2}S_{3313} & \sqrt{2}S_{3312} \\ \sqrt{2}S_{2311} & \sqrt{2}S_{2322} & \sqrt{2}S_{2333} & 2S_{2323} & 2S_{2313} & 2S_{2312} \\ \sqrt{2}S_{1311} & \sqrt{2}S_{1322} & \sqrt{2}S_{1333} & 2S_{1323} & 2S_{1313} & 2S_{1312} \\ \sqrt{2}S_{2111} & \sqrt{2}S_{2122} & \sqrt{2}S_{2133} & 2S_{2123} & 2S_{2113} & 2S_{2112} \end{bmatrix} \quad (14)$$

with:

$$S_{ijkl} = S_{jikl} = S_{ijlk} = S_{klij} \quad (15)$$

Basically, SMA presents two well-defined crystallographic phases, i.e., austenite and martensite. Martensite is a phase that is easily deformed, reaching large strains (~8%), and in the absence of stress, is stable only at low temperatures; in addition, it can be induced by either stress or temperature.

The basic properties of SMAs are the shape memory effect, pseudoelasticity, as well as other properties such as the acquired and two-way shape memory effect, damping capacity and fatigue life. Some of the commonly used SMAs are reviewed by chemical composition and thermomechanical properties. The effects that different processing techniques have on their properties are also discussed. The kinematics associated with the martensitic phase transformation in a single crystal is described for a cubic to tetragonal and cubic to monoclinic transformation, and the lattice invariant strain by plastic slip is discussed [26].

When the martensitic transformation takes place, numerous physical properties are modified. During the transformation, a latent heat associated with the transformation is absorbed or released based on the transformation direction. The forward, austenite-to-martensite transformation is accompanied by the release of heat corresponding to a change in the transformation enthalpy (exothermic phase transformation). The reverse, martensite-to-austenite transformation is an endothermic phase transformation accompanied by absorption of

thermal energy. For a given temperature, the amount of heat is proportional to the volume fraction of the transformed material.

In [27], using the local-density approximation, calculating the Hellmann-Feynman forces, and applying the direct method, the phonon-dispersion relations of cubic austenite, trigonal *R*, orthorhombic and monoclinic martensitic phases of the NiTi intermetallic compound have been derived. The orthorhombic structure, in turn, shows a shear low-frequency mode favoring a martensitic phase. The structures of NiTi phases are well known. At slightly above room temperature this material transforms martensitically from the parent austenite cubic phase to a monoclinic martensitic phase [27]. The martensitic transformation is accompanied by a macroscopic shape change of the crystalline sample. Depending on how the martensitic transformation is provoked, the alloy exhibits different properties such as shape memory or superelasticity. Several diffraction measurements report the structure of the martensitic phase [28-31]

For cubic austenite NiTi the tight-binding band structure has already been presented in [32]. The linear combination of atomic orbitals method was used in [33]. The electronic structure of the monoclinic phase was calculated in [34-37].

2.2. Symmetry cases of Nitinol crystallographic phases

We present the elasticity matrix for the crystallographic phases of Nitinol.

For the trigonal crystallographic structure, the matrix [S] has the expression:

$$[S] = \begin{bmatrix} C_{11} & C_{12} & C_{13} & 0 & -\sqrt{2}C_{15} & 0 \\ C_{12} & C_{11} & C_{13} & 0 & \sqrt{2}C_{15} & 0 \\ C_{13} & C_{13} & C_{33} & 0 & 0 & 0 \\ 0 & 0 & 0 & C_{44} & 0 & 2C_{15} \\ -\sqrt{2}C_{15} & \sqrt{2}C_{15} & 0 & 0 & C_{44} & 0 \\ 0 & 0 & 0 & 2C_{15} & 0 & C_{11}-C_{12} \end{bmatrix} \quad (16)$$

In this case, the eigenvalues are:

$$\begin{aligned} \lambda_1 &= \frac{1}{2} \left[C_{11} + C_{12} + C_{33} + \sqrt{(C_{11} + C_{12} - C_{33})^2 + 8C_{13}^2} \right] \\ \lambda_2 &= \frac{1}{2} \left[C_{11} + C_{12} + C_{33} - \sqrt{(C_{11} + C_{12} - C_{33})^2 + 8C_{13}^2} \right] \\ \lambda_3 = \lambda_6 &= \frac{1}{2} \left[C_{11} - C_{12} + C_{44} + \sqrt{(C_{11} - C_{12} - C_{44})^2 + 16C_{15}^2} \right] \\ \lambda_4 = \lambda_5 &= \frac{1}{2} \left[C_{11} - C_{12} + C_{44} - \sqrt{(C_{11} - C_{12} - C_{44})^2 + 16C_{15}^2} \right] \end{aligned} \quad (17)$$

and the matrix of eigenvectors is:

$$[X] = \begin{bmatrix} \frac{1}{\sqrt{2}} \sin \alpha & \frac{1}{\sqrt{2}} \cos \alpha & \frac{1}{\sqrt{2}} \cos \beta & 0 & \frac{1}{\sqrt{2}} \sin \beta & 0 \\ \frac{1}{\sqrt{2}} \sin \alpha & -\frac{1}{\sqrt{2}} \cos \alpha & -\frac{1}{\sqrt{2}} \cos \beta & 0 & -\frac{1}{\sqrt{2}} \sin \beta & 0 \\ \cos \alpha & \sin \alpha & 0 & 0 & 0 & 0 \\ 0 & 0 & 0 & \cos \beta & 0 & \sin \beta \\ 0 & 0 & -\sin \beta & 0 & \cos \beta & 0 \\ 0 & 0 & 0 & -\sin \beta & 0 & \cos \beta \end{bmatrix} \quad (18)$$

where:

$$\begin{aligned} \sin \alpha &= \frac{|\lambda_2 - C_{11} - C_{12}|}{\sqrt{2C_{13}^2 + (\lambda_2 - C_{11} - C_{12})^2}} \\ \cos \alpha &= \frac{|\lambda_1 - C_{11} - C_{12}|}{\sqrt{2C_{13}^2 + (\lambda_1 - C_{11} - C_{12})^2}}; \\ \sin \beta &= \frac{|C_{11} - C_{12} - \lambda_3|}{\sqrt{(C_{11} - C_{12} - \lambda_3)^2 + 4C_{15}^2}}; \\ \cos \beta &= \frac{|C_{11} - C_{12} - \lambda_4|}{\sqrt{(C_{11} - C_{12} - \lambda_4)^2 + 4C_{15}^2}} \end{aligned} \quad (19)$$

The matrix of the spectral decomposition will be:

$$[E_1] = \begin{bmatrix} \frac{1}{2} \sin^2 \alpha & \frac{1}{2} \sin^2 \alpha & \frac{1}{2\sqrt{2}} \sin 2\alpha & 0 & 0 & 0 \\ \frac{1}{2} \sin^2 \alpha & \frac{1}{2} \sin^2 \alpha & \frac{1}{2\sqrt{2}} \sin 2\alpha & 0 & 0 & 0 \\ \frac{1}{2\sqrt{2}} \sin 2\alpha & \frac{1}{2\sqrt{2}} \sin 2\alpha & \cos^2 \alpha & 0 & 0 & 0 \\ 0 & 0 & 0 & 0 & 0 & 0 \\ 0 & 0 & 0 & 0 & 0 & 0 \\ 0 & 0 & 0 & 0 & 0 & 0 \end{bmatrix} \quad (20)$$

$$[E_2] = \begin{bmatrix} \frac{1}{2} \cos^2 \alpha & \frac{1}{2} \cos^2 \alpha & -\frac{1}{2\sqrt{2}} \sin 2\alpha & 0 & 0 & 0 \\ \frac{1}{2} \cos^2 \alpha & \frac{1}{2} \cos^2 \alpha & -\frac{1}{2\sqrt{2}} \sin 2\alpha & 0 & 0 & 0 \\ -\frac{1}{2\sqrt{2}} \sin 2\alpha & -\frac{1}{2\sqrt{2}} \sin 2\alpha & \sin^2 \alpha & 0 & 0 & 0 \\ 0 & 0 & 0 & 0 & 0 & 0 \\ 0 & 0 & 0 & 0 & 0 & 0 \\ 0 & 0 & 0 & 0 & 0 & 0 \end{bmatrix} \quad (21)$$

$$[E_3] = \begin{bmatrix} \frac{1}{2} \cos^2 \beta & \frac{1}{2} \cos^2 \beta & 0 & 0 & \frac{1}{2\sqrt{2}} \sin 2\beta & 0 \\ \frac{1}{2} \cos^2 \beta & \frac{1}{2} \cos^2 \beta & 0 & 0 & \frac{1}{2\sqrt{2}} \sin 2\beta & 0 \\ 0 & 0 & 0 & 0 & 0 & 0 \\ 0 & 0 & 0 & \sin^2 \beta & 0 & \frac{1}{2} \sin 2\beta \\ -\frac{1}{2\sqrt{2}} \sin 2\beta & -\frac{1}{2\sqrt{2}} \sin 2\beta & 0 & 0 & \sin^2 \beta & 0 \\ 0 & 0 & 0 & \frac{1}{2} \sin 2\beta & 0 & \cos^2 \beta \end{bmatrix} \quad (22)$$

$$[E_4] = \begin{bmatrix} \frac{1}{2}\sin^2\beta & -\frac{1}{2}\sin^2\beta & 0 & 0 & \frac{1}{2\sqrt{2}}\sin 2\beta & 0 \\ -\frac{1}{2}\sin^2\beta & \frac{1}{2}\sin^2\beta & 0 & 0 & -\frac{1}{2\sqrt{2}}\sin 2\beta & 0 \\ 0 & 0 & 0 & 0 & 0 & 0 \\ 0 & 0 & 0 & \cos^2\beta & 0 & -\frac{1}{2}\sin 2\beta \\ \frac{1}{2\sqrt{2}}\sin 2\beta & -\frac{1}{2\sqrt{2}}\sin 2\beta & 0 & 0 & \cos^2\beta & 0 \\ 0 & 0 & 0 & -\frac{1}{2}\sin 2\beta & 0 & \sin^2\beta \end{bmatrix} \quad (23)$$

Particular cases:

a) In the case of the cubic crystallographic structure:

$$C_{12}=C_{13}; \quad C_{33}=C_{11}; \quad C_{44}=C_{11}-C_{12}; \quad C_{15}=0 \quad (24)$$

$$[S] = \begin{bmatrix} C_{11} & C_{12} & C_{12} & 0 & 0 & 0 \\ C_{12} & C_{11} & C_{12} & 0 & 0 & 0 \\ C_{12} & C_{12} & C_{11} & 0 & 0 & 0 \\ 0 & 0 & 0 & C_{44} & 0 & 0 \\ 0 & 0 & 0 & 0 & C_{44} & 0 \\ 0 & 0 & 0 & 0 & 0 & C_{44} \end{bmatrix} \quad (25)$$

The eigenvalues are:

$$\begin{aligned} \lambda_1 &= C_{11} + 2C_{12}; & \lambda_2 &= \lambda_3 = C_{11} - C_{12} \\ \lambda_4 &= \lambda_5 = \lambda_6 = C_{44} \end{aligned} \quad (26)$$

The matrix of eigenvectors is:

$$[X] = \begin{bmatrix} 1/\sqrt{3} & -1/\sqrt{6} & 1/\sqrt{2} & 0 & 0 & 0 \\ 1/\sqrt{3} & -1/\sqrt{6} & -1/\sqrt{2} & 0 & 0 & 0 \\ 1/\sqrt{3} & 2/\sqrt{6} & 0 & 0 & 0 & 0 \\ 0 & 0 & 0 & 1 & 0 & 0 \\ 0 & 0 & 0 & 0 & 1 & 0 \\ 0 & 0 & 0 & 0 & 0 & 1 \end{bmatrix} \quad (27)$$

The matrix of the spectral decomposition will be:

$$[E_1] = \begin{bmatrix} 1/3 & 1/3 & 1/3 & 0 & 0 & 0 \\ 1/3 & 1/3 & 1/3 & 0 & 0 & 0 \\ 1/3 & 1/3 & 1/3 & 0 & 0 & 0 \\ 0 & 0 & 0 & 0 & 0 & 0 \\ 0 & 0 & 0 & 0 & 0 & 0 \\ 0 & 0 & 0 & 0 & 0 & 0 \end{bmatrix} \quad (28)$$

$$[E_2] = \begin{bmatrix} 2/3 & -1/3 & -1/3 & 0 & 0 & 0 \\ -1/3 & 2/3 & -1/3 & 0 & 0 & 0 \\ -1/3 & -1/3 & 2/3 & 0 & 0 & 0 \\ 0 & 0 & 0 & 0 & 0 & 0 \\ 0 & 0 & 0 & 0 & 0 & 0 \\ 0 & 0 & 0 & 0 & 0 & 0 \end{bmatrix} \quad (29)$$

$$[E_4] = \begin{bmatrix} 0 & 0 & 0 & 0 & 0 & 0 \\ 0 & 0 & 0 & 0 & 0 & 0 \\ 0 & 0 & 0 & 0 & 0 & 0 \\ 0 & 0 & 0 & 1 & 0 & 0 \\ 0 & 0 & 0 & 0 & 1 & 0 \\ 0 & 0 & 0 & 0 & 0 & 1 \end{bmatrix} \quad (30)$$

b) In the case of monoclinic crystallographic structure:

$$[S] = \begin{bmatrix} C_{11} & C_{12} & C_{13} & 0 & 0 & C_{16} \\ C_{12} & C_{22} & C_{23} & 0 & 0 & C_{26} \\ C_{13} & C_{23} & C_{33} & 0 & 0 & C_{36} \\ 0 & 0 & 0 & C_{44} & C_{45} & 0 \\ 0 & 0 & 0 & C_{45} & C_{55} & 0 \\ C_{16} & C_{26} & C_{36} & 0 & 0 & C_{66} \end{bmatrix} \quad (31)$$

The eigenvalues are:

$$\begin{aligned} \lambda_4 &= \frac{1}{2} \left[C_{44} + C_{55} + \sqrt{(C_{44} + C_{55})^2 + 4C_{45}^2} \right] \\ \lambda_5 &= \frac{1}{2} \left[C_{44} + C_{55} - \sqrt{(C_{44} + C_{55})^2 + 4C_{45}^2} \right] \end{aligned} \quad (32)$$

and $\lambda_1, \lambda_2, \lambda_3, \lambda_4$ are the roots of the equation:

$$\lambda^4 - I_1\lambda^3 + I_2\lambda^2 - I_3\lambda + I_4 = 0 \quad (33)$$

where I_k is the sum of the diagonal minors of k degree obtained by cutting the fourth and the fifth columns and rows in matrix $[S]$.

c) In the case of orthorhombic crystallographic structure:

$$[S] = \begin{bmatrix} C_{11} & C_{12} & C_{13} & 0 & 0 & 0 \\ C_{12} & C_{22} & C_{23} & 0 & 0 & 0 \\ C_{13} & C_{23} & C_{33} & 0 & 0 & 0 \\ 0 & 0 & 0 & C_{44} & 0 & 0 \\ 0 & 0 & 0 & 0 & C_{55} & 0 \\ 0 & 0 & 0 & 0 & 0 & C_{66} \end{bmatrix} \quad (34)$$

The eigenvalues are:

$$\lambda_4 = C_{44} \quad \lambda_5 = C_{55} \quad \lambda_6 = C_{66} \quad (35)$$

and $\lambda_1, \lambda_2, \lambda_3$ are the roots of the equation:

$$\lambda^3 - I'_1\lambda^2 + I'_2\lambda - I'_3 = 0 \quad (36)$$

where I'_k is the sum of the diagonal minors of k degree obtained by cutting the last three columns and rows in matrix $[S]$.

3. The analytical expression for the staple compression force

The stress vector can be written:

$$(\sigma) = \sum_i (\sigma_i) \quad (37)$$

where:

$$(\sigma_i) = [E_i] \cdot (\sigma) \quad (38)$$

Therefore, the specific deformation energy is:

$$U = \frac{1}{2} \cdot \sum_{(i)} \frac{1}{\lambda_i} \cdot (\sigma_i)' \cdot (\sigma_i) \quad (39)$$

The orthopedic staple can be modeled as a bar which has an initial shape. When temperature increases it suffers deformations, changing its shape. Taking into account mechanically considerations, the deformation can be accepted as being caused by an exterior force which is applied to the free extremity. Thus, an increase of temperature, ΔT produces a displacement of the free extremity, Δw . The same displacement can be produced by a force (ΔP) which is applied in the free extremity. In fact, the force (ΔP) is a force to be applied in the free extremity.

The total deformation energy is:

$$U = \frac{1}{2} \cdot \sum_{(i)} \frac{1}{\lambda_i} \cdot \iiint (D) (\sigma_i)' \cdot (\sigma_i) \cdot dv \quad (40)$$

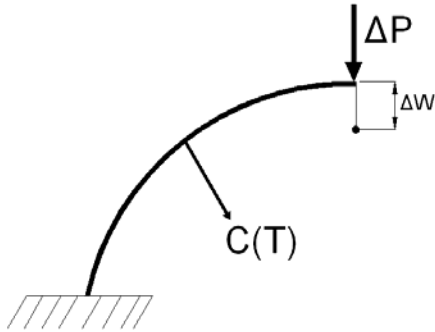


Fig.1. The loading schema for the Nitinol staple

According to the Castigliano theorem energy, the derived strains of an elastic body compared with force value ΔP seam with the displacement projection of the application point of the direction force (fig.1).

$$\Delta w = \frac{\partial U}{\partial (\Delta P)} \quad (41)$$

In the case of small deformations we can accept that the stress developed in the staple are proportional to the variation force ΔP . In these conditions, we can write:

$$\Delta w = \Delta P \cdot \sum_{(i)} \frac{1}{\lambda_i} \cdot \iiint (D) (e_i)' \cdot (e_i) \cdot dv \quad (42)$$

where:

$$(e_i) = \frac{\partial (\sigma_i)}{\partial (\Delta P)} \quad (43)$$

The vectors (e_i) depend only of the staple shape. The triple integrals which occur in the relation (42) depend on the temperature, but in a measure much smaller than the eigenvalues.

$$J_i = \iiint (D) (e_i)' \cdot (e_i) \cdot dv \quad (44)$$

Therefore the integrals can be considerate constants. In this case, by passing to the limit, the relation becomes:

$$\dot{w} = \dot{P} \cdot \sum_{(i)} \frac{1}{\lambda_i} \cdot J_i \quad (45)$$

Taking into account the small volume of the staple, it can be considered that the temperature reached is given by the law:

$$\dot{T} = c(T_e - T) \quad (46)$$

where c is a coefficient which depends on the material thermal conductivity of the staple. T_e is the temperature of outdoors. The temperature variation on time is:

$$T = T_e - (T_e - T_i) \cdot e^{-c(t-t_i)} \quad (47)$$

T_i = initially temperature of staple;

t_i = initially value of time;

The eigenvalues λ_i of the elasticity matrix depend on the temperature and on the value $e^{-c(t-t_i)}$

$$\lambda_i = \lambda_i(T_e; T_i; e^{-c(t-t_i)}) \quad (48)$$

Experimentally, it is demonstrated that the staple deformation is produced with constant speed: $w = cst$, (Fig.11). In [38] were tested three Nitinol wire specimens: a commercially available superelastic (W_1) wire and two shape memory wires with their nominal A_f points were 35°C (W_2) and 40°C (W_3), respectively. They showed typical superelastic hysteresis loops under the restraint condition at 40°C . After the wire was given a 1.0 mm maximum deflection at 32°C , the changes in the recovery force against the deflection were examined when the wire was subjected to the following temperature changes:

- (1) $32^\circ\text{C} - 40^\circ\text{C} - 32^\circ\text{C}$
- (2) $32^\circ\text{C} - 23^\circ\text{C} - 32^\circ\text{C}$

Furthermore, the changes in the recovery force were pursued during the deflection change from 1.0 to 0mm at each temperature successively after the temperature was changed. Also, it is demonstrated that the dependence of recovery force function on temperature is linear.

Developing in factors series in function of term $e^{-c(t-t_i)}$ the functions of the proper values and keeping only the first order term, the relation (45) becomes:

$$P = f(T_e; T_i) \cdot e^{-c(t-t_i)} \quad (49)$$

The variation in time of the compression force exerted by the staple is:

$$P = P_i + \frac{1}{c} \cdot f(T_e; T_i) \cdot (1 - e^{-c(t-t_i)}) \quad (50)$$

where: P_i is the exerted force at the initial moment t_i .

4. Experimental studies for the Nitinol staple

In order to determine the law of variation for the compression force which can be developed by the Nitinol staple as a function of variable environmental temperature and also to validate the compression potential of the staple through constant pressure at the temperature of the human body, we developed an experimental stand (Fig.2).

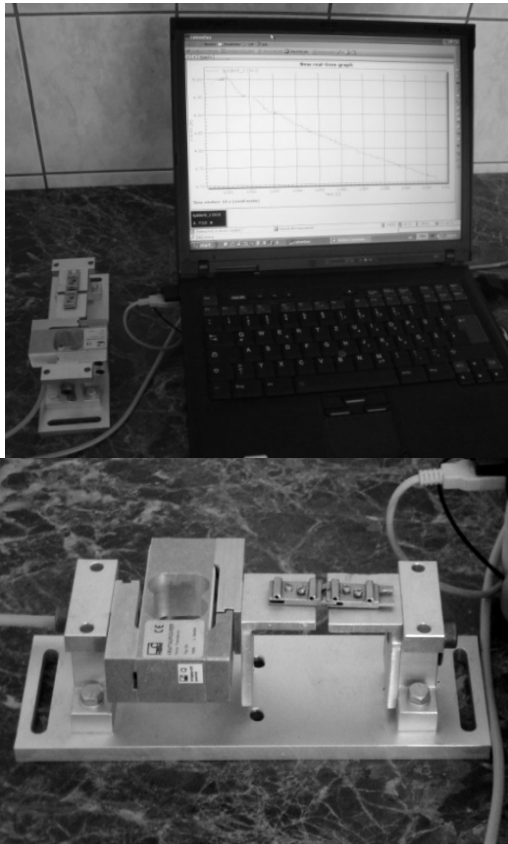


Fig.2. Experimental stand

The experimental stand is made from:

- Experimental device used to mount the modular adaptive implant;
- Spider 8 – a numerical acquisition system, 12 bits resolution, used to measure mechanical parameters, such as: forces, mechanical stresses, pressures, accelerations, velocities, displacements, temperatures. The acquisition

system contains specialised modules for measuring various mechanical parameters (Fig.3.).

-S2-100N force transducer, 0.1% linearity, Hottinger type. The transducer works for compression-traction and is based on four strain gauges in full configuration with temperature compensation. The strain gauges are mounted on a fibreglass base reinforced with fenolic resin. The response is situated in the [-200...+250] °C temperature domain.

-FLIR B200 termographic camera,

-IBM ThinkPad R5 notebook.

The Nitinol staple was stored for 15 minutes in NaCl liquid solution, 30% concentration, at -20°C in a freezer. At this temperature the material of the staple enters in martensitic phase and the lateral pins of the staple are parallel. Having this shape, the staple was extracted from the NaCl solution and was easily inserted in special channels of the two implant modules fixed in the device.

The staple was then left to attain room temperature (29°C), thereby compressing the two modules.

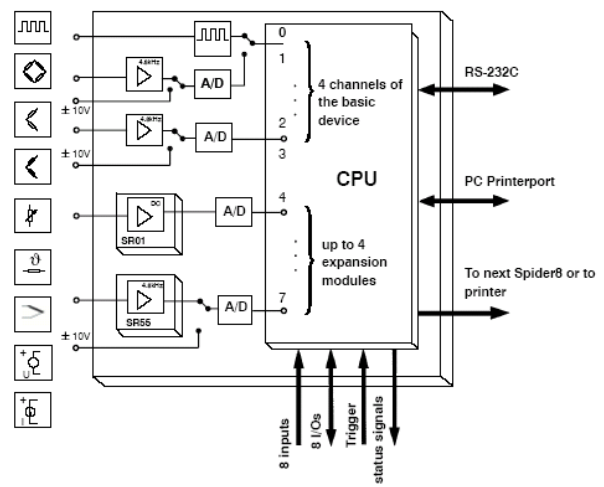


Fig. 3. Spider 8- the connection scheme for the processing and input modules

Afterwards, a jet of hot air was blown onto the staple increasing his temperature in different stages: first, to 31°C, in a time period of 120 sec, then, to 35°C in a time period of 120 sec and, finally, to 37°C, the temperature of the human body. The hot air jet was then stopped and after the staple returned to room temperature it was extracted from the modular implant.

Finally, we obtained the force-temperature plot (based on 65000 acquired pairs of data). One can observe a maxim value of 54 N which corresponds to 37°C temperature for which the material of the staple entered in the second phase: cubic austenite (Fig.4).

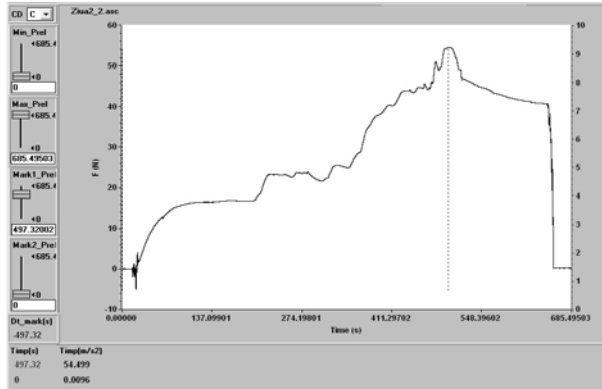


Fig.4 The compression force function on time

In order to correlate the staple deformation with the developed compression force, the temperature increase has been controlled with the aid of a termographical camera ThermoCam Flir B200.

The ThermoCam workflow is (Fig.5):

1. Images in infrared or/and digital pictures are taken;
 2. The images are moved from Termacam to PC;
 3. Using the FLIR QuickReport software, the analysis of the images is made;
 4. The Report for infrared images is realized.
- Several successive infrared frames have been taken during the experiment (Fig. 6).

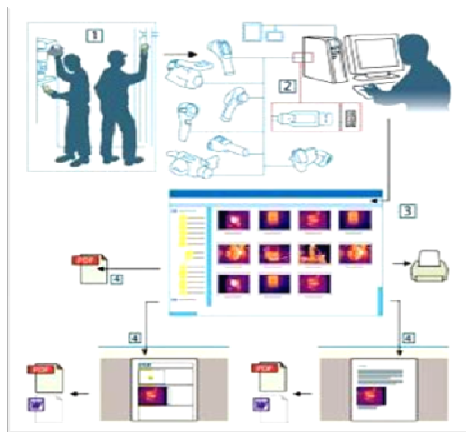


Fig. 5. ThermoCam workflow.

Afterwards, these pictures have been processed and analysed. For the image in which the Nitinol staple reached 37⁰ C we have obtained temperature diagrams by transferring in Microsoft Excel the database corresponding to the temperatures of each pixel of the A1 area (Fig.7). The corresponding graphics are presented in Fig.8.

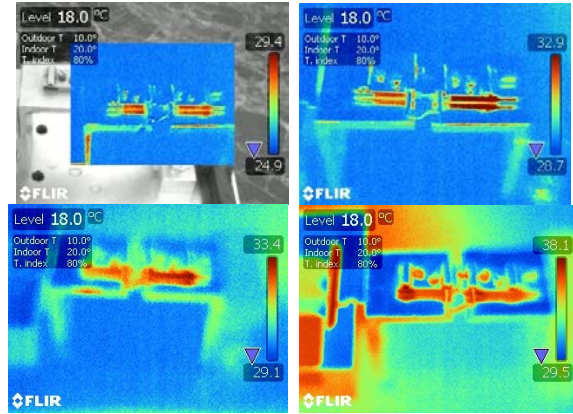


Fig.6. Several images taken with termographical camera

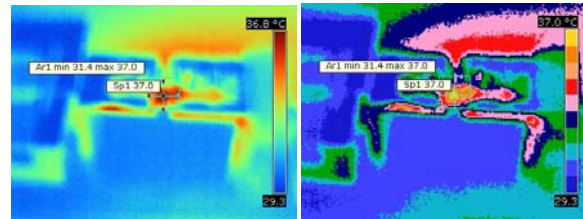


Fig.7. Image corresponding to 37⁰ C temperatures in two variants: a) red –blue palette b) Rain palette

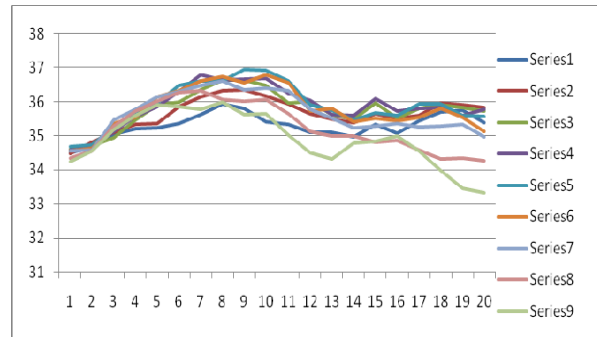


Fig.8. The temperature variation in the pixels situated on 9 lines of the Ar₁ area

Using the SIMI Motion software, the kinematical parameters of the both extremities of the staple were obtained. The Block schema of Simi Motion video analysis method is presented in Fig.9. Two successive positions of staple deformation process are presented in Fig.10. In Figures 11, the displacement diagram [mm], as functions of time, for the left point is presented. One can be observed that the dependence displacement-time is linear. This observation was used for the determination of the compression force theoretical expression.

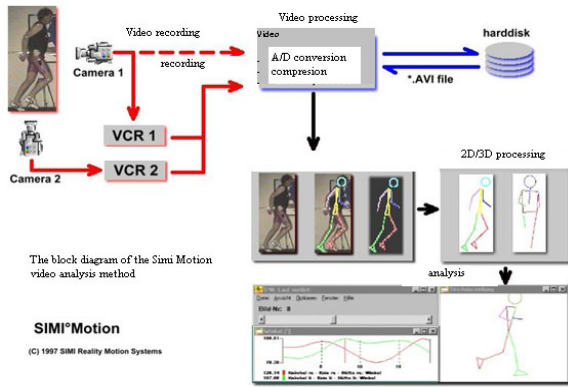


Fig.9. The Block schema of the Simi Motion video analysis method

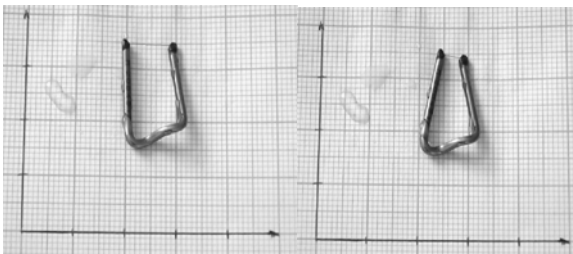


Fig.10. Two successive positions of staple deformation process

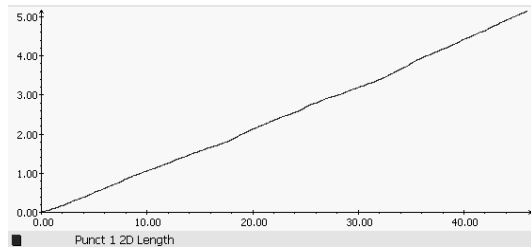


Fig.11. The displacement diagram for the left extremity of the staple

5. Discussions

The elasticity matrixes for the crystallographic phases of Nitinol are presented. The eigenvalues depend on the values of the elastic constants, but the eigenvectors are, in part, independent of the values of the elastic constants. We consider that the staple finishes its deformation when the difference between its temperature and room temperature is $\leq 1^{\circ}C$. In this hypothesis, the coefficient c can be determined with the relation:

$$c = \frac{\ln(T_e - T_i)}{\Delta t} \tag{51}$$

where Δt is the staple deformation time.

Experimentally, we can see that $\Delta t = 45\text{sec}$, corresponding to the interval $[-20; 29]^{\circ}C$ of temperature variation (Fig.11). In this case, the resulted value for c is $0,086\text{sec}^{-1}$. This value corresponds to the studied staple, so, taking into account the concrete experimental conditions, it is a constant for this product. Any other product made from Nitinol will have other value for c . The experimental diagram presented in fig.4 shows the stages of the compression force variation corresponding to the stages of the temperature variation (Table 1).

Table 1. Compression force values.

Temperature variation ($^{\circ}C$)	Compression force variation (N)	Values for $f(T_e - T_i)$ (N)
-20.....29	0.....17	$f(29;-20)=17$
29.....31	17.....24	$f(31;29) = 7$
31.....35	24.....44	$f(35;31)=20$
35.....37	44.....54	$f(37;35)=10$

Using the values for $f(T_e - T_i)$ as input data in the relation (50), we made a numerical simulation in Maple12 and we obtained the graphic presented in Fig.12. For the numerical simulation, we respected the same temperature increasing stages as in the experimental case. This explains the allure of the numerical graphic. For first temperature increase, from $-20^{\circ}C$ to $29^{\circ}C$, the force variation is nonlinear, and for the other three stages we observe that the force increasing is less than 10 N for a temperature increasing with $2^{\circ}C$, the force variation is linear. For constant temperatures, the force remains constant.

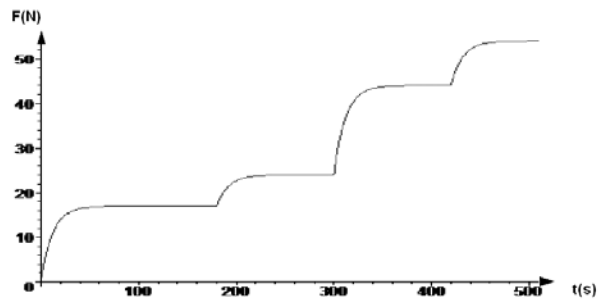


Fig.12 The numerical graphic.

The diagram force-displacement proves the maximum of the compression force (54 N) is obtained in the Nitinol staple at the body temperature, $37^{\circ}C$. This properties of the Nitinol staple allows its using in orthopedic applications, like simple orthopedic implants, or adaptive modular implants (Fig.13).

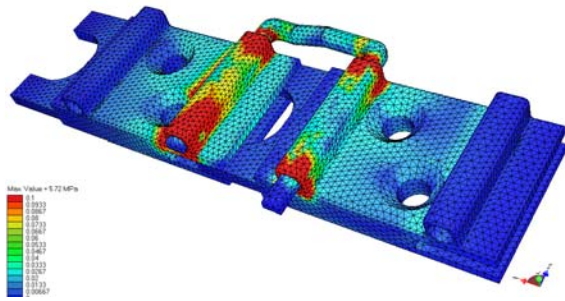


Fig.13. Two modules connected by a Nitinol staple

The proposed adaptive modular implant is a bone plate assembly made from two Titanium modules and a Nitinol staple [39]. The shape memory staple is, initially, in their opened shape. Through heating, this staple tends to the original shape, the closed shape, developing a constant compressing force of 56 N at the 37°C body temperature. This implant represents a superior solution in the process of the fractured bones osteosynthesis over the conventional implants known so far, due to the following advantages:

- the possibility of mounting the Nitinol staple to the modules situated near the fracture hotbed enables the stabilization of the implants and the good union of the bone fractures, a key element in the healing process;
- due to constant pressure exerted, it provides the compaction of the fractures fragments.
- the small sizes of the modules enable the surgeon to use minimally invasive surgery, with following advantages:

- reduction of soft tissues destruction;
- elimination of intra-operator infections;
- reduction of blood losses;
- reduction of post-operator infection risk;
- reduction of the healing time;

The video capture analysis used for experimental studies is a fast, accurate kinematical study method. The data acquired through the experimental methods can be used to corroborate the experimental kinematical parameters with kinematical parameters obtained using various analytical or numerical simulations in order to confirm a certain mechanical model.

Acknowledgements

This research work was supported by CNCSIS-UEFISCSU, grant 86/2007, Idei_92

References

- [1] C. M. Friend, N. B. Morgan, Professional Engineering Publishing Ltd., UK, p. 1, 1999.
- [2] M. Ryhänen, J. Kallioinen, J. Tuukkanen, Professional Engineering Publishing Ltd. P. 53, 1999.
- [3] A. R. Pelton, D. Stöckel, T.W. Duerig, Mater Sci Forum **327–328**, 63 (2000).
- [4] D. Mantovani, Journal of the Minerals, Metals and Materials Society **52**, 36 (2000)
- [5] T. M. Duering, A. Pelton, D. Stockel, Metall **50**, 569 (1996).
- [6] D. C. Lagoudas, O. K. Rediniotis, M. M. Khan, Proceedings of the 4th International Workshop on Mathematical Methods in Scattering Theory and Biomedical Technology, Perdika, 1999.
- [7] T. M. Duering, A. Pelton, D. Stockel, Materials Science and Engineering A, **273–275**, 149 (1999).
- [8] S. A. Shabalovskaya, Journal de Physique IV, **5/2(8):C8.1199–C8.1204**, 1995
- [9] Raghuvir Singh, B. Narendra, Dahotre. J Mater Sci: Mater Med **18**, 725 (2007).
- [10] K. W. Yeung, R. W. Poon, P. K. Chu, et al., J Biomed Mater Res A., **82(2)**,403 (2007).
- [11] Jorma Ryhanen, Antti Leminen, Timo Jamsa, et al. A novel treatment of grade III acromioclavicular joint dislocations with a C-hook implant. Arch Orthop Trauma Surg **126**, 22 (2006).
- [12] D. J. Wever, J. A. Elstrodt, A. G. Veldhuizen, et al.. Eur Spine J **11**, 100 (2002).
- [13] Evangelia Petoumeno, Maya Kislyuk, Hildegard Hoederath, et al.. J Orofac. Orthop, **69**, 411 (2008).
- [14] P. Sevilla, F. Martorell, C. Libenson, et al. J Mater Sci: Mater Med **19**, 525 (2008).
- [15] H. Z. Morawiec, Z. H. Lekston, K. F. Kobus et al. J. Mater. Sci: Mater Med **18**, 1791 (2007).
- [16] W. Xu, T. G. Frank, G. Stockham, et al.. Annals of Biomedical Engineering., **27**, 663 (1999).
- [17] Y. Ng, S. M. Shimi, N. Kernohan, et al. Surg Endosc **20**, 311 (2006).
- [18] L. Kelvin, Phil. Trans. R. Soc. **166**, 481 (1956).
- [19] S. C. Cowin, M. M. Mehrabadi, , Quarterly Journal of Mechanics and Applied Mathematics, **40(4)**, 451 (1987).
- [20] M. M., Mehrabadi, S. C. Cowin, Quarterly Journal of Mechanics and Applied Mathematics, **43**, 15 (1990).
- [21] T.C.T.Ting, Quarterly Journal of Mechanics and Applied Mathematics, **40(3)**, 431 (1987).
- [22] G. F. Smith, R. S., Rivlin, Transactions of the American Mathematical Society, **88**, 175 (1958).
- [23] J. Rychlewski, J. Zhang, . Anisotropy degree of elastic materials. Arch. Mech. **47(5)**, 697 (1989).
- [24] S. Sutcliffe, Journal of Applied Mechanics, **59**, 761 (1992).
- [25] P. S., Theocaris, E. Philippidis, Archives of Mechanics, **41(5)**, (1989)
- [26] E. Patoor, D. Lagoudas, P. Entchev, L. Brinson, X. Gao, Mechanics of Materials, **38**, 391 (2006).
- [27] K. Parlinski, Physical Review B **66(064307)**, 1 (2002).
- [28] R.F. Hehemann, G. D. Sandrock, Scr. Metall. **5**, 801 (1971).
- [29] G. M. Michal, R. Sinclair, Acta Crystallogr., Sect. B: Struct. Crystallogr. Cryst. Chem. **37**, 1803 (1981).
- [30] W. Büchner, R. Gotthardt, A. Kulik, F. Staub, J. Phys. F: Met. Phys. **13**, L77 (1983).
- [31] Y. Kudoh, M. Tokonami, S. Miyazaki, K. Otsuka, Acta Metall. Mater. **33**, 2049 (1985).
- [32] R. Bruinsma, Phys. Rev. B **25**, 2951 (1982).

- [33] G.L. Zhao, B.N. Harmon, *Phys. Rev. B* **48**, 2031 (1993).
- [34] G. Bihlmayer, R. Eibler, A. Neckel, *J. Phys.: Condens. Matter* **5**, 5083 (1993).
- [35] Bihlmayer, R. Eibler, A. Neckel, *Philos. Mag. B* **73**, 51 (1996).
- [36] S. E. Kul'kova, V.E. Egorushkin, V.V. Kalchikhin, *Solid State Commun.* **77**, 667 (1991).
- [37] S. E. Kul'kova, K. A. Beketov, V.E. Egorushkin, O. N. Muryzhnikova, *J. Phys. IV* **5**, C8 (1995).
- [38] Kotaro Yanaru, Kazunori Yamaguchi, Hiroshi Kakigawa, Yoshio Kozono, Temperature- and Deflection- Dependences of Orthodontic Force with Ni-Ti Wires, *Dental Materials Journal* **22**(2), 146 (2003).
- [39] D. Tarniță, D. N. Tarniță, L. Hacman, C. Copiluş, C. Berceanu, *Rom J Morphol Embryol*; **51**, 315 (2010).

*Corresponding author: dtarnita@yahoo.com